INTERANNUAL VARIATIONS IN THE RETREAT OF THE NOTHERN SEASONAL CAP OF MARS USING COMPUTER VISION.

P. J. Acharya[1] *(pruthvi1@yorku.ca)*, **I. B. Smith**[1] *(ibsmith@yorku.ca)*, ***W. Calvin***[2] *(wcalvin@unr.edu)*,[1]*York University, Toronto, Ontario, Canada,* [2]*Nevada University, Reno, Nevada*

Introduction: One of the largest features on Mars is the Northern Seasonal Polar Cap (NSPC), with can cover up to 12% of the surface seasonally [1]. The NSPC condenses up to 25% of the atmosphere during wintertime and releases it during springtime [2], leading to a major change in the global atmospheric pressure and composition. Intense atmospheric activities are often seen originating near the cap's edge during springtime [3,4]. These activities have been seen to reach very close to the equator, indicating a large amount of material being moved in and out of the polar region. For these reasons, it's critical to understand the NPSC's recession to understand the past, present, and future Martian climate.

The focus of this work was to update and extend the previously published results [4] using an automated approach. We were able to track the cap's edge at a higher temporal resolution than previously possible [4] and were able to add new MYs that haven't been analyzed previously. With the enhanced dataset, we determined the seasonal variation in the recession rate for each year, interannual observations, and mid-season changes that were previously undetected.

MARCI Observations: We used large-scale visual observations from the Mars Color Imager (MARCI) from MY 29 to MY 35. Each observation is a mosaic of 12-13 images taken within 24 hours, each image covers ~27.7º of the northern polar region (Fig 1A) [4]. For each MY, we tracked the cap until L_s = 70º; around this time the cap's edge reaches the polar layered deposits and it's difficult to distinguish between the seasonal and residual ice.

Automated Tracking: Using Python and an open-sourced computer vision library called OpenCV, we automated outlining the cap and fitting an ellipse of best fit. Our method relied on using the Hue, Saturation, Value (HSV) color format, where important properties of color are decoupled into their own channels. Using this format, we empirically determined the best upper and lower H, S, and V bounds that best outlined the seasonal cap and ignored the water-ice clouds (Figs 1A, B). Then we fitted an initial ellipse best fit (Fig 1B) and used a simple filtering algorithm to remove any outlier outline points, which were caused by imaging artifacts (Figs 1D) and dust storms (Fig 1e), to get a filtered ellipse fit. We record the average axis, and the area of the ellipse fits while using over 99% of the MARCI observations. Our new method was significantly faster and produced a higher temporal resolution curve compared to the previous approaches using the same MARCI dataset (Figs 2B, C, D) [3,4].

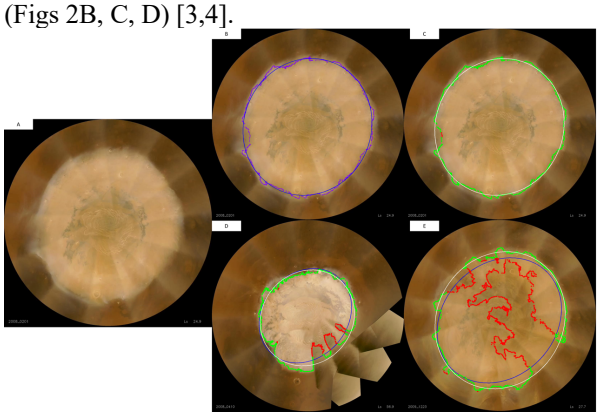

Figure 1: *MARCI mosaic at MY 29 L_s = 24.9º.* ***A.*** *Full color MARCI mosaic.* ***B.*** *MARCI mosaic with the initial ellipse fit (Blue) and outline points (Purple).* ***C.*** *MARCI mosaic with the filtered ellipse (White), outlines points that passed the filtering algorithm (Green), and points that failed (Red).* ***D.*** *MARCI mosaic during an imaging artifact at MY 29 L_s = 56.9°.* ***E.*** *MARCI the mosaic at MY 30 L_s = 27.7º during a dust storm.*

Validation: We validated our method by comparing results to those from Calvin et al. (2015) by looking at the outline (Fig 2A) and recession rates for MY 29 to MY 31 (Figs 2B-2D). Both methods produced similar outlines; however, Calvin et al. (2015)'s outline is smoother than our outline. Additionally, both methods produced similar seasonal recession rates and latitude extent, except for MY 29 where our method is ~2.5° larger than Calvin et al. (2015)'s observations. When we compare our results to Cantor et al. (2010), who used similar MARCI observations and methods to find the seasonal recession rates for MYs 28 and 29, our method closely matches their results (Fig 2B).

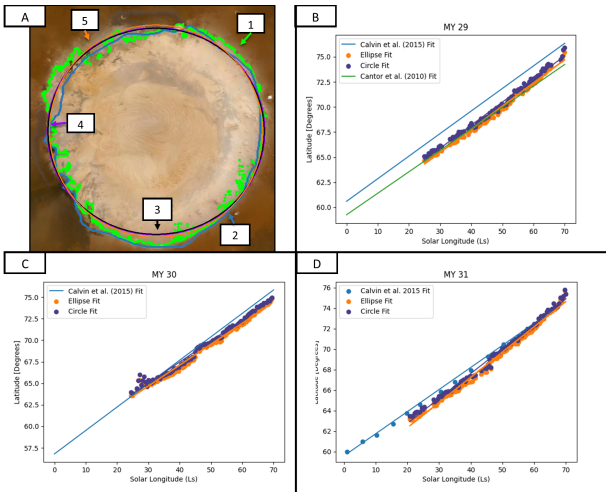

Figure 2: A. *Comparison between our results and those from Cantor et al. (2010) and Calvin et al. (2015) for a MARCI mosaic at MY 29 at L_s 62.5. A: (1) our outline in green, (2) Calvin et al. (2015)'s outline in blue, (3) Calvin et al. (2015)'s outline in purple, (4) our circle of best fit using the HSV method in black, (5) our ellipse of best fit using the HSV method in orange.* ***B:*** *Comparisons of the three survey's latitudinal extents over MY 29. Calvin et al. (2015) in blue; Cantor et al. (2010) in green); our ellipse of best fit in orange; our circle of best fit in purple.* ***C and D:*** *Same as B but for MY 30 and MY 31.*

Results: We used a line of best fit, a 7th order polynomial fit and its first derivative to analyze the multi-year average and individual MY recession curves. We found that most MYs behaved very similar to each other, with an average recession rate of ~0.24º/L_s. Most MYs diverged from the linear rate between L_s = ~35º and L_s = ~50º, transiting from the annual minimum to maximum recession rate (Figs 3C, D). Also, the latitude recession rate is slower early in the season and faster later in the season.

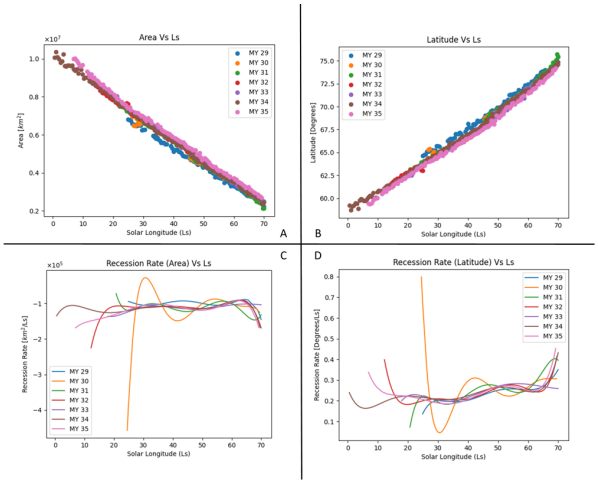

Figure 3: *Comparison of all MYs from L_s = 0º to L_s = 70º* ***A.*** *Area change (in km²).* ***B.*** *Average axis change (in °N).* ***C.*** *First derivative for the 7th order area fit (in km²/L_s).* ***D.*** *First derivative for the 7th order average axis fit (in °/L_s).*

Sudden Latitude Increasing Event: We find that MY 30 experiences a sudden latitude increase beginning L_s = ~44º, where the cap shrinks by ~0.8° by L_s = ~45º. Following this, the cap returns to its linear fit by L_s = ~51º; however, the recession rate is ~55% faster than before this event (Fig 4A). In addition, there are dust storms seen moving southwards just before this increase (Fig 4B). It should be noticed that we believe that this is the second sudden increasing event, as near the start of the observations we noticed that cap's latitude is converging towards the linear fit. Additionally, there are intense storms seen over the entire region; however, due to the lack of observations we are unable to see the initial increase, so our interpretation will focus on the latter increase.

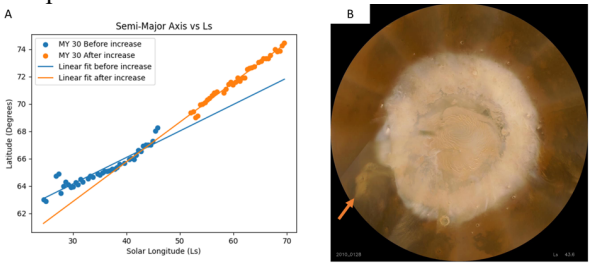

Figure 4: ***A.*** *shows the latitude vs L_s for MY 29 with the linear fit before (Blue) and after (Orange) sudden increase.* ***B.*** *shows the latitude vs L_s for MY 30 with the linear fit before (Blue) and after (Orange) sudden increase.* ***C.*** *shows a dust storm occurring at MY 29 L_s = 51.1º around the time of the increase.* ***D.*** *shows a dust storm occurring at MY 30 L_s = 43.6º around the time of the increase.*

We believe that the sudden increase may be caused by a major sublimation event and katabatic winds flowing away from the pole (Fig 5b). After this, recession halts because the cap's edge is sufficiently far away from the Sun's maximum latitude reach and won't resume until the Sun catches up to the cap's edge (Fig 5c). Once the Sun reaches the cap's edge, recession resumes but it is enhanced by katabatic winds, which are stronger than before and known to increase sublimation rates [5,6,7,8] (Fig 5d).

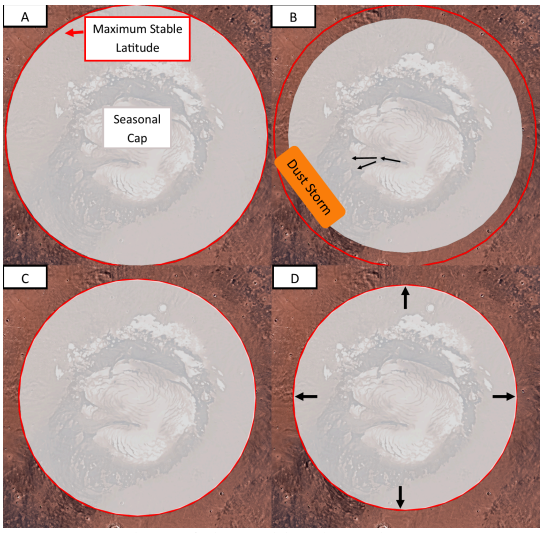

Figure 5: *Timeline of the sudden latitude increasing event. The blue circle represents the seasonal cap, the red circle represents the maximum latitude where the cap is stable or the maximum latitude reach of the Sun, and the black arrows represent the katabatic winds.* ***A.*** *Cap receding solely due to solar radiation and closely following the maximum stable latitude.* ***B.*** *A major sublimation event decreases the size of the cap and seasonal katabatic winds formed during this time, causing the storms seen around this time.* ***C.*** *Recession halts because the cap is well within the stable latitude region and katabatic winds are sufficient to continue recession.* ***D.*** *Maximum stable latitude reaches the cap's edge and recession resumes but is enhanced by katabatic winds.*

Effects of the Global Dust Storms: The seasonal cap following the MY 28 and MY 34 global dust storms deviated significantly from the MY that did not follow the storms. MY 29's cap was significantly smaller, and the area recession rate was significantly slower, until L_s = 40°, than the other MYs. MY 35's cap was slightly larger and receded slightly faster throughout the entire observational period. We believe that the abnormal behavior of the seasonal cap following the global storm is due to the difference in the behavior of the storm.

The MY 28 storm first appears at L_s = ~262° [9], just as the NPSC reached maximum extent [1], and the storm has mostly died out by L_s = ~322° [9]. On the other hand, the MY 34 storm first appears much earlier, around L_s = ~185° [9], before the NPSC began to form [9], and quickly died out by L_s = ~220° [9], about midway through the formation period [1].

For the early MY 28 global storm, we have hypothesized three explanations by which the global storm can cause a smaller NPSC. The polar vortex may be displaced during the storm [1], this would cause parts of the NPSC to sublimate faster than others [1], resulting in a smaller NPSC following the storm. Another possible explanation is that as the storm dies out, dust is deposited on the surface, lowering the surface albedo, and the cap sublimates faster, resulting in a smaller cap. There could be a combination of the previously discussed explanations; asymmetries originally arose from the displaced polar vortex could reduce the surface albedo at the margins of the cap, enhancing sublimation and accelerating recession prior to the start of our observations.

To test this, we measured the displacement of the center of the ellipse with respect to the geographical north pole (Fig 6A), the eccentricity of the ellipse (Fig 6B), azimuth of the ellipse (Fig 6C), and the average brightness of the outer edge of the NPSC (Fig 6D) for all MYs. It's expected that early in the season; MY 29's cap should have a large displacement, a highly eccentric cap, and/or be a darker cap than other MYs. Contrary to our prediction, prior to L_s = 40°, MY 29 has a smaller displacement and the outer edge of the NPSC is the brightest. Interesting, during this period, MY 29 is the most eccentric cap and the largest azimuth value, suggesting some sort of polar vortex displacement. However, these together put our explanation to question.

Considering MY 34, because the storm died quickly, there was ~100 L_s between the ending of the storm and the start of the recession. This gives time for the polar vortex to correct itself and the atmospheric dust levels to return to background levels. Also, previous work showed that during the MY 28 global dust storm, the average temperature decreased by ~10°K [10]. Assuming similar conditions during the MY 34 storm, we hypothesize that a cooler surface is present following the MY 34 global storm, enhancing the cold trapping rate, and resulting in a larger cap. The larger cap would sublimate faster early in the season from lower latitude, where the sun is the most intense. This agrees with our observations for MY 35 which has the highest early-season recession rate.

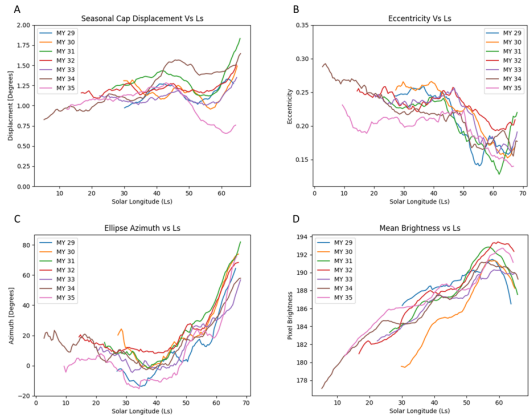

Figure 6: Ellipse fit parameters to test the moving polar vortex's effect on the NPSC retreat, with a moving average of 10 to reduce noise. ***A:*** *Displacement of the ellipse fit with respect to the geographical north pole vs L_s.* ***B:*** *Eccentricity vs L_s.* ***C:*** *Azimuth angle vs L_s, negative values represent longitude values west of 0°E.* ***D:*** *Mean brightness of the outer 3° vs L_s.*

Future Work: Going forward, we plan to develop a dynamic color detector that can better accommodate regional dust storm; current static bound fails during those storms. We also plan on further testing our explanation for the sudden latitude increasing event and effect of the global dust storm using numerical models and new observations. In addition, we plan on using our method on the Southern Seasonal Polar Cap using similar MARCI mosaics and comparing the two polar caps.

Acknowledgments: We gratefully acknowledge the support of the NSERC Discovery grant to IBS and from the Technology for Exo-Planetary Science (TEPS) CREATE grant to PA

References: [1] Piqueux, S. et al. (2015) Icarus, 251, 164–180. [2] Tillman, J. E.et al. (1993) JGR 98(E6), 10963. [3] Cantor, B. A.et al. (2010) Icarus, 61–81. [4] Calvin, W. M. et al. (2015) Icarus181–190. [5] Smith, I. B. et al. (2013) JGR 1835–1857. [6] Smith, I. B. and Spiga, A. (2018) Icarus, 308, 188–196. [7] Bramson et al. (2019 JGR 124, 1020–104. [8] Spiga, A. and Forget, F. (2009) JGR, 114. [9] Wolkenberg, P. et al. (2020) JGR, 125(3). [10] Plesa, A.-C. et al. (2016) JGR, 121(10), 2166–2175.